Impact of artificially matured organic matter on the dielectric and elastic properties of compacted shales

Matthieu Cauchefert*
Curtin University
Department of Exploration Geophysics
26 Dick Perry Avenue, Kensington, WA
matthieu.cauchefert@postgrad.curtin.edu.au

Matthew Josh
CSIRO
Earth science and resource engineering
26 Dick Perry Avenue, Kensington, WA
matthew.josh@csiro.au

Lionel Esteban
CSIRO
Earth science and resource engineering
26 Dick Perry Avenue, Kensington, WA
lionel.esteban@csiro.au

Stephanie Vialle
Curtin University
Department of Exploration Geophysics
26 Dick Perry Avenue, Kensington, WA
Stephanie.vialle@curtin.edu.au

Maxim Lebedev
Curtin University
Department of Exploration Geophysics
26 Dick Perry Avenue, Kensington, WA
M.Lebedev@exchange.curtin.edu.au

Jeremie Dautriat
CSIRO
Earth science and resource engineering
26 Dick Perry Avenue, Kensington, WA
Jeremie.Dautriat@csiro.au

Joel Sarout
CSIRO
Earth science and resource engineering
26 Dick Perry Avenue, Kensington, WA
Joel.Sarout@csiro.au

Bruce Maney
CSIRO
Earth science and resource engineering
26 Dick Perry Avenue, Kensington, WA
Bruce.Maney@csiro.au

SUMMARY

Unconventional gas shale resources recently became a standard in the American oil and gas industry and are studied throughout the world. However Gas shales are still poorly characterised with respect to other reservoir rock types. The organic matter (OM) in organic shales is rarely taken into account in all its complexity and variability. This study focuses on the influence of OM maturity on the dielectric and elastic response of shale using a hydrous pyrolysis process to increase their maturity. We then incorporated the OM in a shale-like mineral matrix that was artificially compacted under control. Elastic properties and their anisotropy were measured during compaction while dielectric measurements were acquired post-compaction. The results showed that OM affects the onset of the liquid/plastic transition of compacting sediment. The immature OM lessens the development of P-wave anisotropy. On the other end, mature OM strongly decreases the imaginary dielectric permittivity at low frequencies while it increases electrical conductivity.

Key words: Shale, Organic matter, P-wave, Dielectric, Anisotropy, Hydrous pyrolysis

INTRODUCTION

Despite recent advances in petroleum technologies for exploration, prospection and enhanced oil/gas recovery in unconventional tight gas shale reservoirs, this sedimentary rock type -the most abundant on Earth- still remains the least studied and poorly understood. Among the many reasons to that under-representation of shales in scientific studies we can quote its very low permeability, its chemical reactivity with liquids or the difficulty to preserve natural samples (Ewy, 2015). OM adds another level of complexity as its content, type and maturity will gauge the gas/oil storage capacity of the shale, influence most of its physical responses from various tools (lab, logs and models) and affect transport and mechanical properties of the formation(s), especially in near well conditions.

Unfortunately, OM is way too often restricted to its weight fraction content represented by the total organic carbon (TOC). Hence its real impact on the physical-chemical properties of shales is over-simplified. For instance, it was shown that shale elastic response and its anisotropy are considerably affected by OM maturity (Emmanuel et al., 2016), its orientation and distribution (Vernik and Nur, 1992; Sayers, 2013). Likewise Delle Piane et.al. (2017) demonstrated that the presence of highly mature graphene leads to unusually high conduction and dielectric permittivity within a shale, and Josh et.al. (2016) substantiate this finding with compacted synthetic shales and numerical simulation that both non-conductive and conductive OM can play a role.

The intrinsic complexities of natural shales (mineralogy, compaction-diagenesis history, heterogeneity…) and the various parameters/properties involved in shale studies bring strong barriers to properly understand them. Through the study of artificial shales we can create and analyse samples with great repeatability and focus on one or two variable of interest.
In this paper, the variables in our samples are the organic content and its maturity. We collected immature peat samples and we developed a method to simulate natural maturation through hydrous pyrolysis and then incorporate immature and mature OM in synthetic shales that are subsequently compacted to study their dielectric and elastic behaviour. We will present how OM and maturity affect the liquid/plastic transition of compacting sediments, the development of elastic and dielectric anisotropy and the conductivity of shales.

EXPERIMENTAL METHODS

In this study, the experimental workflow is subdivided into three major components. First of all, OM is prepared before incorporation into the sample mixture. The synthetic samples are then compacted. Thereafter they are sliced in different directions to undergo dielectric testing.

Base materials

The choice of the different constituents of the artificial samples is crucial to the quality of the data to be acquired. Synthetic samples are not meant to be identical to natural ones but rather are a simplification of natural shales. All their mineralogical and petrophysical parameters can be controlled and we can focus on one or two variables. The components must be chosen according to the properties that will be measured and the natural characteristics to be reproduced. In the present case, dielectric and elastic properties of natural shales give us constraints for the sample compositions. A homogeneous mineral matrix that remains steady is required to highlight the influence of the considered variable: the organic phase. The resulting matrix has to feature vertical transverse anisotropy typical of shale formations and silt and clay-sized particles to reproduce the morphology of shales grain contacts. It must also be rich in clay minerals as the clay/water interactions play an important role in the dielectric response of shales. In addition, strong electrical conductor such as pyrite must be avoided to not overshadow the dielectric behaviour of OM.

Hillier (2006) gathered an extensive database of mineralogical compositions of European shale formations of various ages (Cambrian to Quaternary). He computed the average composition of the collection. The mineral composition of our samples is based on this data. The resulting samples do not match any particular formation but instead represents an 'average' mineralogy that best suits the purpose of reproducing the dielectric and elastic behaviour of a typical shale. After rounding up and eliminating the minerals present in minor proportions, we came up with a mineralogy reduced to four groups: Quartz, Feldspar, Carbonate and Clay. The dominant minerals for the Feldspar and Carbonate groups have been selected: Potassium feldspar (Orthoclase) and calcite, respectively. Finally, kaolinite is chosen preferred to represent the Clay group due to a readily availability and a lower potential for swelling in presence of water. The proportion of each mineral for each sample of the study is detailed in table 1.

The organic material used for this study is a Canadian sphagnum peat moss from Nova Scotia. This material was chosen to reproduce OM containing type III kerogen (gas prone) and because it is the earliest precursor with the lowest possible maturity. Hence it represents the level 0 of maturity and the subsequent process of artificial maturation can yield a wide range of maturities from the same initial material. The Von Post classical method is described by Stanek and Silc (1977). This tool assesses the humification of a peat sample. The degree of humification represents the degradation state of the peat, mainly due to microbial decomposition. As humification goes on, the elemental composition of peat changes towards immature kerogen ones. Namely the proportion of carbon increases at the expanse of the oxygen fraction that diminishes whereas hydrogen tends to remain stable (Delicato, 1996). After examination, the OM at our disposition proves to be a poorly humified peat of rank H2. This corresponds to a high atomic O/C ratio of approximately 0.8 and an H/C ratio between 0.9 and 1.

Sample name	Dry mineral composition (wt%)				
	Quartz	K-Feldspar	Calcite	Clay (Kaolinite)	Organic (immature /mature peat)
lean	20	10	10	60	0
M0	18.2	9.1	9.1	54.7	8.9
M1	18.3	9.1	9.1	54.7	8.8

Table 1: Mineral composition of each sample. M0 stands for maturity 0, the sample containing immature peat whereas M1 is the sample containing artificially matured peat. The lean sample is the inorganic witness sample.

Organic matter preparation and maturation

The peat was initially dried at 85^0C for a week and was then ground into a fine powder so it can easily be mixed homogeneously into the mineral matrix. About 90g of this powder was isolated to experience artificial maturation. To obtain a mature sample chemically similar to kerogen found in shale source rocks, a hydrous pyrolysis system has been developed. The principle of such system is to heat under pressure and in the presence of water an organic sample in a closed environment. Indeed it was shown that pyrolysis of immature source rocks carried out in the presence of water gives products with a chemical composition the closest to natural hydrocarbons (T.Barth, 1999). Moreover, several studies insist on the importance of the mineral matrix on the maturation of OM. Clay minerals especially have a great ability to adsorb organic compounds. The chemical interactions between OM and clays occur at this adsorbed interface. The greater the specific surface area of the clay, the greater is the resulting catalysis effect. Thus swelling clays shown in multiple studies to be the major catalyst (Wu et al., 2012). The relationship between the clay and the organic phase during maturation is further emphasized by the study of Rahman et al. (2017) where a greater contact between the two phases resulted in greater hydrocarbon production through pyrolysis.

This information gathered in the literature helped to define the requirements of an OM maturation system. The choice of a closed system containing 90% peat and 10 % swelling clays (bentonite) with the presence of water was retained. We used a pressure vessel CF-0.2L from KDinstrument with a ceramic lining equipped with a pressure gauge and a pressure relief valve. A picture of the vessel can be seen on Figure 1-a. The vessel was placed in an oven at 250^0C. The temperature was set at the upper end of the temperature

range where the vessel can be operated safely to maximize the rate of thermal OM cracking. Under those conditions, the water vapour pressure generated equals to 4MPa. The sample was left several days in the closed heated vessel and was then left to dry at 85^0C. Finally we ground the obtained material to incorporate it into the sample the same way the immature peat was, according to the procedure detailed below.

Compaction procedure

At first the dry powder minerals (and possibly OM) are put together. To keep track of the density and porosity during the compaction, the exact amount and density of each initial constituent must be known. The initial minerals must resemble a homogeneous powder. Otherwise, they are ground and/or oven-dried. The density of each constituent is measured using a helium pycnometer. According to the proportion needed for the final sample and the required initial volume, each constituent is weighed with a ±0.01g precision the amount of. Thereafter the constituents are poured in a bowl together and undergo a thorough dry mixing.

Then the pore fluid is prepared from deionised water preliminary degassed for 24h under vacuum. Salts are then added to match the target brine composition. For the present sample set, a standard brine with 15g/L NaCl was used. The brine is then added to the dry mix of minerals. The liquid mix is subsequently stirred for a substantial time. The operator ensures no dry packs of grains remain in the mix. When the slurry visually seems perfectly homogeneous, the mix is stirred further as a precaution. Ideally the mix must have a high water content (>75%) to prevent air bubbles being trapped in the sample.

The mixture is poured into the compaction cell. The cell is equipped with P-wave transducers that record ultrasonic signals in the horizontal, vertical and two different off-axis directions. The theoretical height of the initial sample derived from the volumes of the different constituents is verified using a Vernier calliper. A Linear Variable Differential Transducer (LVDT) is installed on the actuator and will record the shortening, and by extrapolation the volume, of the sample during compaction. Elastic moduli and the ε and δ Thomsen's anisotropy parameters can be computed from the picking of the first P-wave arrival time and the corrected sample dimensions, throughout the compaction process.

The compaction cell is installed under a reaction frame. The compaction is insured by an actuator which is brought into contact with the cell piston. The pore lines are installed and directed towards a scale that records expelled fluid masses. A picture of the cell in operation is reported in Figure 1-b. The load is applied on the sample with a regulator. The operator enters a target value for the stress and a selected stress rate. The regulator then controls through a feedback loop the actuator displacement accordingly. The loading path for the three samples is divided in two phase. An initial pressure of 1MPa is maintained constant over several hours until the sample hits the liquid to plastic limit. The sample is then loaded up to 10MPa of vertical compressive stress at a rate of 3.75MPa/hour.

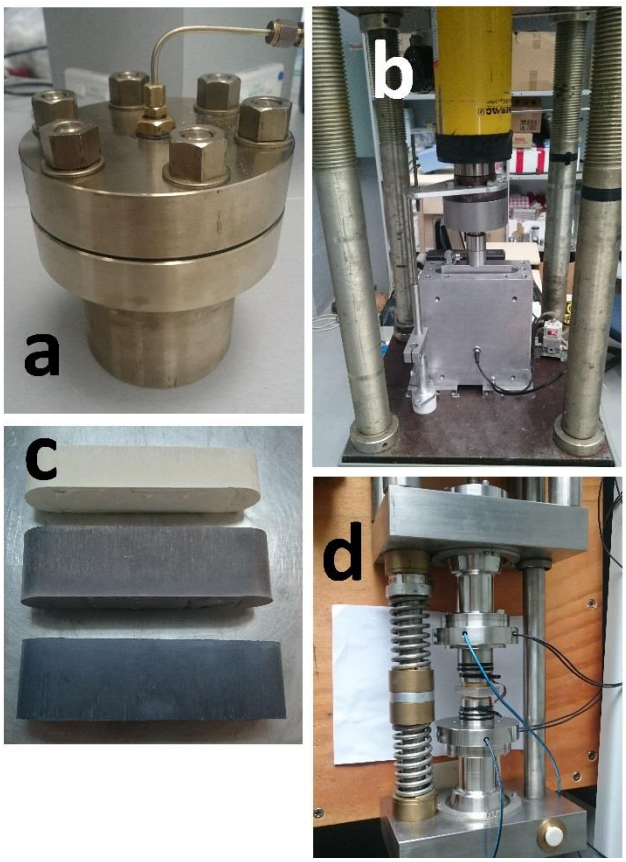

Figure 1: a) Hydrous pyrolysis vessel. b) Compaction cell under the actuator. A transducer cable is visible on the cell wall. c) From top to bottom: sample lean, M0, M1. d) Sample slice in the parallel plate dielectric apparatus

At the end of the compaction experiment the sample can be unloaded rapidly or by steps. The expansion upon unloading – relatively low - can be measured and corresponds to the compressibility of the mineral matrix. The cell is then disassembled and the sample extracted (Figure 1-c). The final weight and volume are measured and are used to double check the density and porosity values measured by the apparatus sensors. Finally the sample is sealed and put in a refrigerator to maintain saturation level before subsequent dielectric testing, explained in the following section.

Dielectric testing

The dielectric relative permittivity εr measures the electrical polarizability of a material under an alternating electric field. It is influenced by conduction and polarisation mechanisms, which can be explained as the translation and the reorientation of charge carriers, respectively. It is heavily frequency-dependent with larger scale processes dominating the dielectric response at low frequency and small scale processes detectable at high frequency. There is a real ε'r and an imaginary ε''r part to the dielectric permittivity. The former can be regarded as a measure of the intensity of the polarization and the latter is related to the work exerted by the different mechanisms.

A vertical and a horizontal slice about 10mm thick are extracted from each of the samples obtained after compaction. The two faces of a slice must be almost perfectly parallel with a constant thickness down to ±0.1mm to ensure a good coupling between the sample and the dielectric equipment. The slice is positioned between the parallel plate and pressed with a very small pressure to form a contact surface as can be seen be seen on Figure 1-d. Next the measurement is run with an Agilent impedance analyser (4294A). The apparatus measures the real and imaginary part of

the dielectric permittivity and can compute the equivalent electrical conductivity. The plates are also equipped with P-wave transducers to get unconfined ultrasonic data. Each slice is tested with direct contact to the parallel plate and through a plastic film. The first configuration gives information about the conduction processes while the second focuses on polarization processes.

RESULTS AND DISCUSSION

The compaction of the three samples was carried out in nearly the same conditions of initial porosity, maximum compressive stress, fluid salinity and loading paths as shown in table 2. The only notable difference is the stabilization time at 1MPa that lasted longer for the lean sample. We can see that each sample has a final unconfined porosity about 2.5% higher than the final porosity under stress, which is attributed to the deformation of the solid phase upon stress release. Despite similar conditions, the final porosity is lower for the lean sample and higher for M1.

Sample name	porosity (%)				maximum vertical stress (Mpa)	pore fluid salinity (g/L)	First phase @1MPa (hours)
	initial	At the end of the first phase	final under stress	final unconfined			
lean (no OM)	79.42	46.7	34.9	37.4	10.2	14.5	11.7
M0	78.99	50.6	36.5	38.8	10.2	15.1	6.5
M1	78.84	50.9	37.2	39.5	10.2	15.3	6.2

Table 2: information summary from the compaction experiments.

The inflection of the porosity curves (Figure 2) at the end of the first phase (constant stress at 1MPa) shows the transition of the sample from a liquid material to a plastic material. The porosity decrease over time is very similar for the two organic samples. On the other hand the lean sample has a slower porosity decrease rate during the 1MPa phase but reaches a lower porosity at the end of the first phase. This is attributed to the fact that the first phase was almost twice as long for the lean sample. However we can see that the inflection of the curve for the lean sample also occurs at a lower porosity than for the organic samples. The two organic samples, on the other hand have very similar behaviour. This suggests that the organic matter plays a role in the transition from a poorly consolidated sediment to a plastic material, regardless of the maturity of that OM.

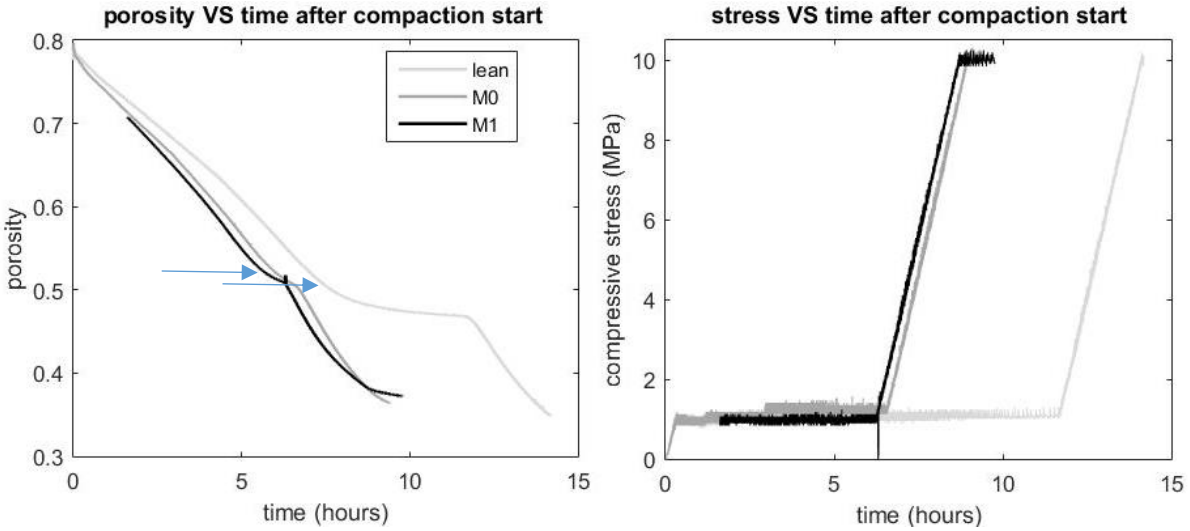

Figure 2: Porosity (left) and compressive stress (right) evolution during the compaction experiments. The arrows show the inflexion of the porosity curve at the end of the liquid phase.

The two phases of compaction are also visible on the ultrasonic data, as shown in Figure 3. The P-wave travel time is affected both by the velocity increase of the compacting material and the distance change between source and receiver, as two of the transducers are embedded in the piston, moving down during compaction.

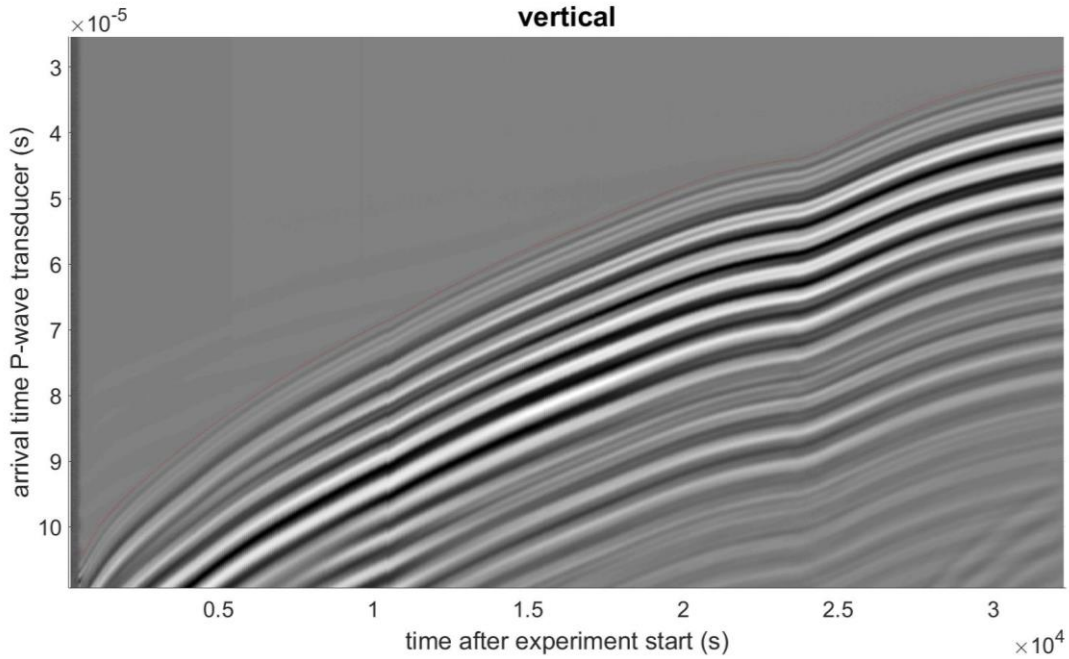

Figure 3: P-wave arrival time profile for a compaction experiment. Here is sample M0, signal propagating vertically. The red line is the picked time for velocity computation.

P-wave velocity is computed from the travel time data. Figure 4 shows the evolution of the P-wave velocity (plain and dashed lines), and the unconfined velocities measured during the dielectric tests (triangles). At the start of the compaction, for all samples, vertical and horizontal velocities are all around 1500 m/s, the velocity of P-waves in water. During the first phase, the velocity increases very slowly when porosity decreases, until the sample hits the liquid/plastic threshold. During the second phase, the velocity increases drastically and elastic anisotropy develops, with the horizontal velocity becoming progressively larger than the vertical velocity, as expected from a compacting clay-rich shale exhibiting a preferential orientation of clay platelets/particles orthogonal to the direction of compaction. Also expected is the fact that the unconfined velocity is lower than its confined counterpart. However, with this Figure, it is difficult to distinguish notable differences between samples.

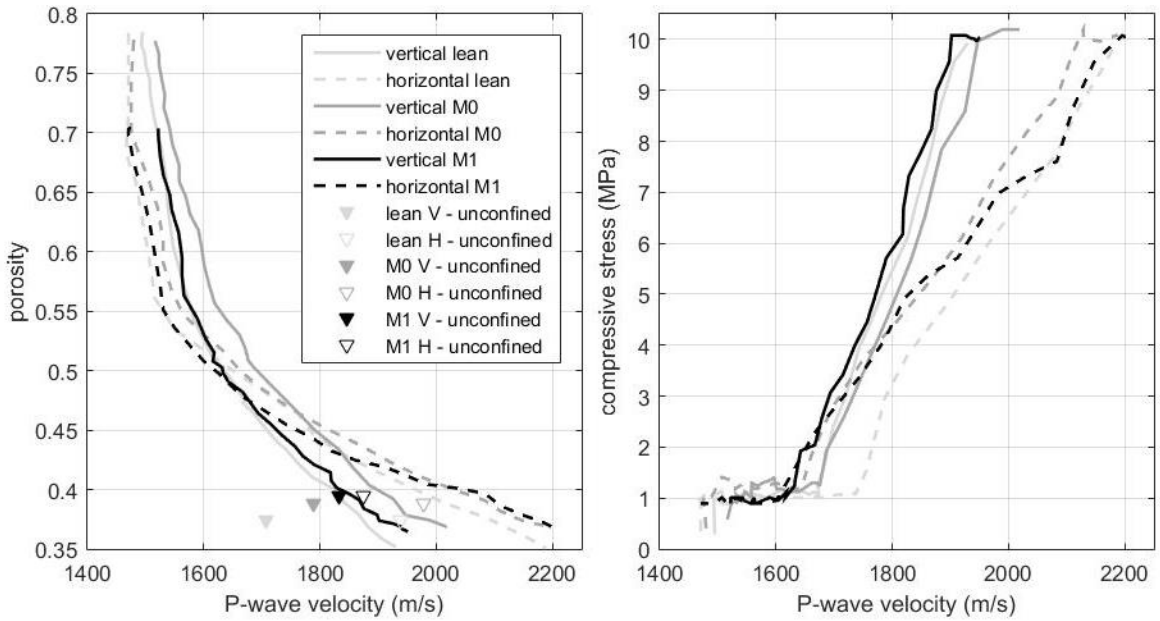

Figure 4: Porosity (left) and compressive stress (right) as a function of P-wave velocity.

In an attempt to clarify this data, we compute Thomsen's P-wave anisotropy parameter ε (Thomsen, 1986) equal to $[Vp(\pi/2)\text{^}2 - Vp(0)\text{^}2]/2 * Vp(0)\text{^}2$ with 0 indicating vertical propagation (slower) and $\pi/2$ indicating horizontal propagation (faster). Although the general trends in the evolution of anisotropy are similar to those of the previous Figures, a few new elements are worth noting. First of all we see both on the porosity and stress plots that M0 develops less anisotropy ($\varepsilon \approx 0.07$) than the other samples whereas the lean sample and M1 reach the same anisotropy by the end of the compaction ($\varepsilon \approx 0.14$). This suggests that the immature OM impedes the development of anisotropy whereas the mature OM had a minor effect. We also note that the unconfined anisotropy of the lean and

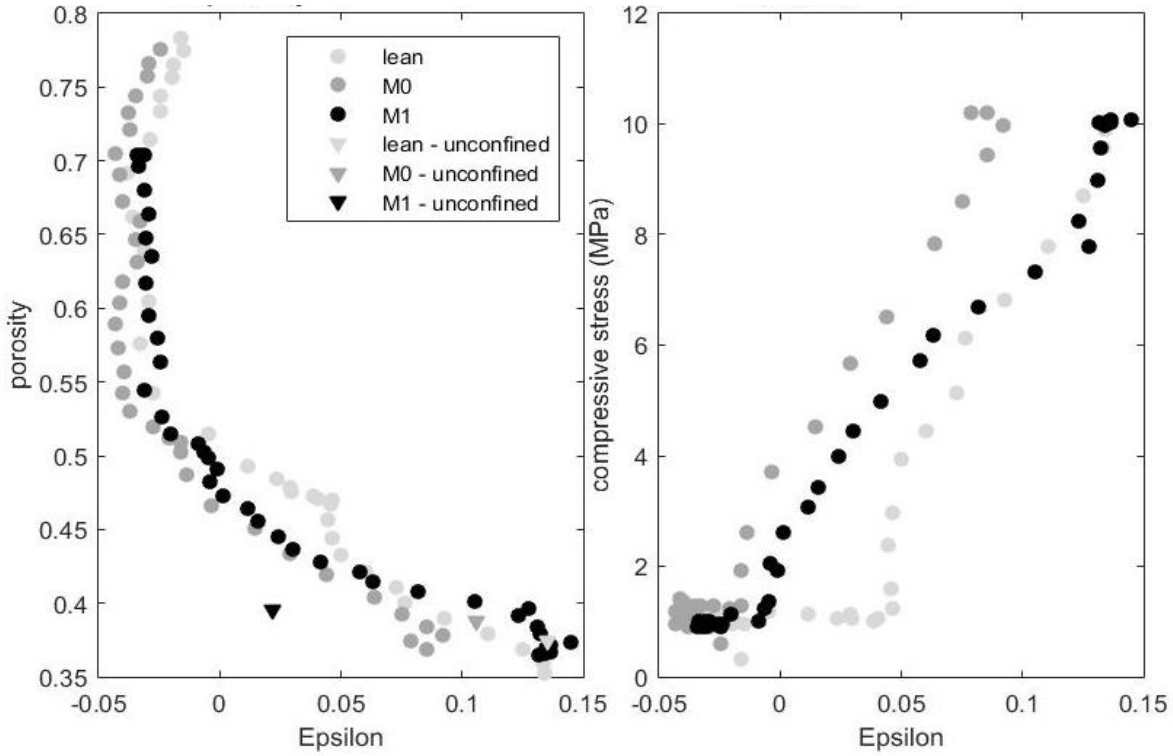

Figure 5: Porosity (left) and compressive stress (right) as a function of Thomsen's anisotropy parameter ε.

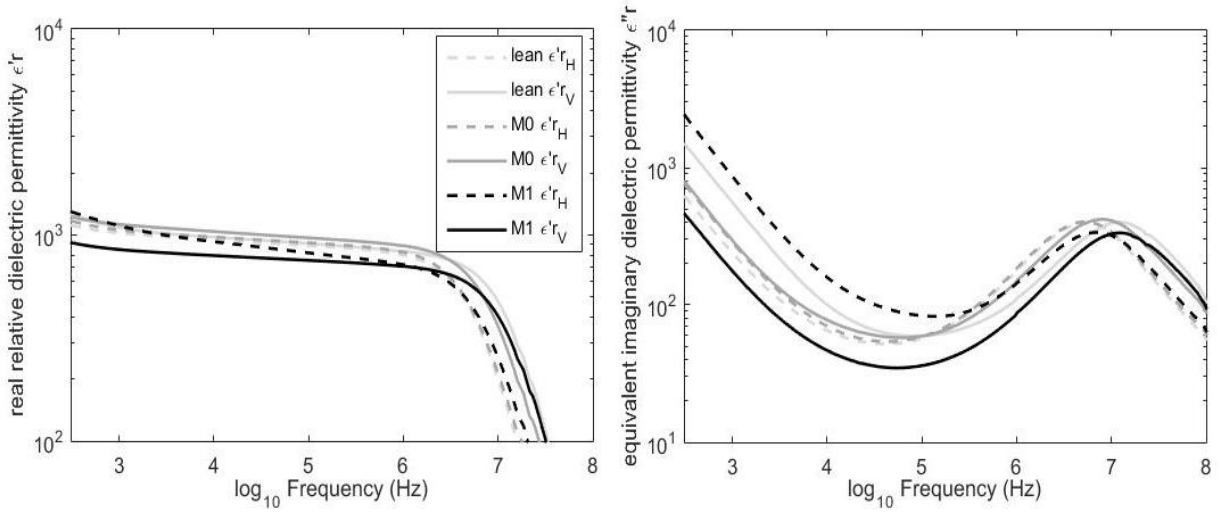

Figure 6: Real (left) and Imaginary dielectric permittivity as a function of the electrical field frequency in the horizontal direction (dashed line) and vertical direction (plain line).

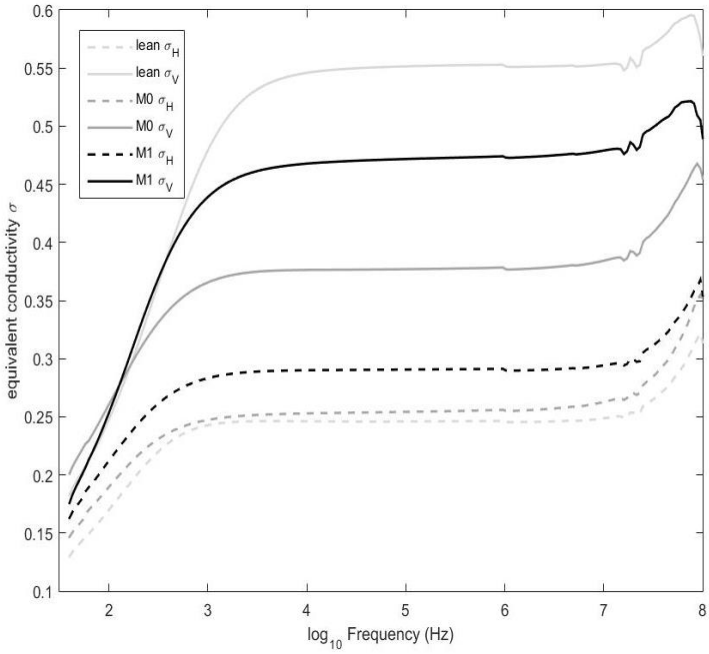

Figure 7: equivalent conductivity as a function of the electrical field Frequency in the horizontal direction (dashed line) and the vertical direction (plain line).

M0 samples is within the trend of the confined values. On the other hand the unconfined anisotropy of M1 is much lower than the confined one, at equivalent porosity. Therefore the more mature organic sample may be more affected by the stress release than the immature and lean samples. Nevertheless the small number of unconfined data points doesn't allow us to draw any definitive conclusion on this aspect.

The dielectric permittivity data do not allow for discriminating among the three sample types: they all exhibit a similar dielectric response, both in terms of real and imaginary parts (Figure 6). However, the equivalent conductivity displays an interesting pattern (Figure 7). Sample M0 is less conductive than M1, both in the horizontal and vertical directions. In other words, as expected, the more carbon rich mature OM is overall a better electrical conductor. Otherwise the horizontal lean sample has a lower conductivity than any of the other samples whereas the vertical lean sample has the greatest conductivity of all. This feature is also visible in Figure 8c, with a conduction anisotropy much higher for the lean sample. Alike what we saw with the P-wave anisotropy of the M0 sample, organic matter appears to reduce the anisotropy of electrical conductivity.

The imaginary dielectric anisotropy (Figure 8b) is similar for all samples above a frequency of 10^5 Hz. But at lower frequency, the imaginary dielectric anisotropy is greater than one for the lean sample, comparable to 1 for M0, and lower than 1 for M1. The imaginary permittivity at these frequencies represents the work exerted by space-charge polarization in larger pores.

This indicates that the space-charge polarization requires more work in the vertical direction for the lean sample but less work for the sample M1, and M0 hasn't preferential orientation.

Finally we can see an increase in the real dielectric anisotropy for M0 and M1 around 10^7 Hz on Figure 8a. This was also observed in another study (Josh et. al., 2016). Yet, unlike our results the inorganic witness sample in that study had a lower anisotropy at that frequency.

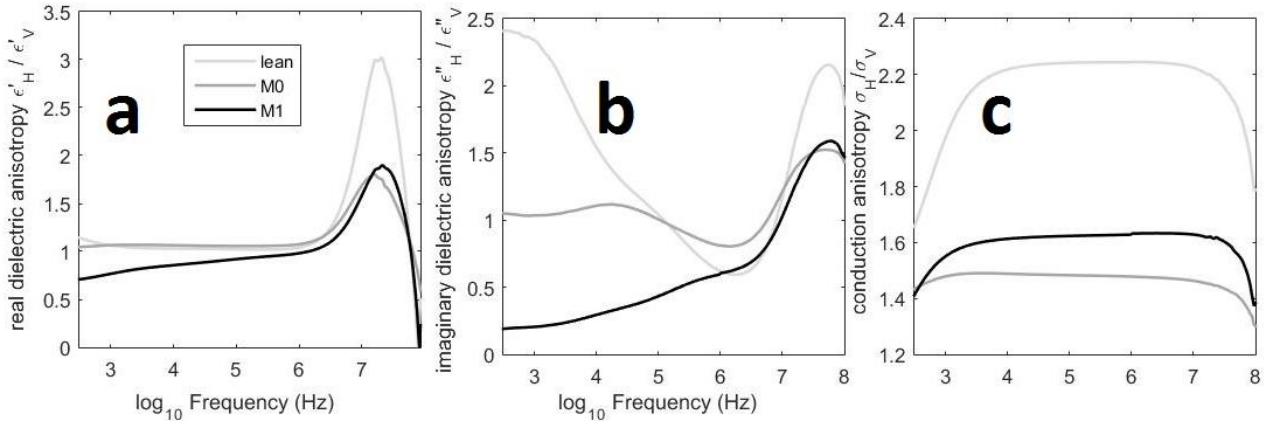

Figure 8: Anisotropy of the real permittivity, imaginary permittivity and the equivalent conductivity for each sample.

CONCLUSION

Our results suggest that the OM, regardless of the maturity, affects the onset of the liquid/plastic transition of compacting sediments. Besides, highly immature peat when compacted in a shale mineral matrix seems to lessen the development of elastic anisotropy, whereas matured peat doesn't. Also organic-rich samples decrease the electrical conductivity anisotropy, and the more mature sample is more conductive than its immature counterpart. Finally, OM appears to strongly influence the imaginary dielectric permittivity at low frequencies, effectively reversing it with increasing maturity.

Nevertheless the results presented in this study have to be interpreted carefully. It is worth highlighting the maturation of the organic phase was done prior to the compaction experiment and was incorporated after drying. Hence the observed behaviour reflects the intrinsic influence of the OM only and in water-saturated conditions. The effects the microcracks produced upon hydrocarbon generation and the hydrocarbon itself aren't present here. Also the slow deposition of the minerals and the OM in natural sediment occurs far differently from the mixing method we used for our sample and must have an impact on elastic anisotropy notably. These additional mechanisms are not accounted for here.

Further analysis such as optical microscopy of thin sections and petrological analysis of the OM is yet to be carried out on these samples. It will help determine the role of OM in the observed dielectric and elastic responses. The computation of Thomsen's anisotropy parameter δ for this dataset is also underway (a parameter that controls the geometry of the wavefront in the transversely isotropic shale). In the continuity of this study, plans for other artificial samples with maturation performed post-compaction, different organic matter types and the presence hydrocarbon-wet OM will help evaluate the importance of OM on petrophysical and geomechanical properties.

ACKNOWLEDGMENTS

I (MC) was supported by Curtin International Postgraduate Research Scholarship and Australian Government Research Training Program Scholarship. This work was partially funded through the CSIRO Shale Rock Physics and Petrophysics (SHARPP) project sponsored by Total. I would also like to thank Sam Battah for his contribution to the design of the cell and Ausama Giwelli for introducing me to compaction experiments.

REFERENCES

Barth, T. (1999). Similarities and differences in hydrous pyrolysis of biomass and source rocks. *Organic Geochemistry*, *30*(12), 1495-1507.

Delle piane, C., J. Bourdet, M. Josh, M. B. Clennell, W. D. A. Rickard, M. Saunders, N. Sherwood, Z. Li, D. N. Dewhurst, M. D. Raven, 2017, Organic matter network in post mature Marcellus Shale: effects on petrophysical Properties, AAPG Bulletin, In Press.

Delicato, D. (1996). *Physical-chemical properties and sorption characteristics of peat* (Doctoral dissertation, Dublin City University).

Emmanuel, S., Eliyahu, M., Day-Stirrat, R. J., Hofmann, R., & Macaulay, C. I. (2016). Impact of thermal maturation on nano-scale elastic properties of organic matter in shales. *Marine and Petroleum Geology*, *70*, 175-184.

Ewy, R. T. (2015). Shale/claystone response to air and liquid exposure, and implications for handling, sampling and testing. International Journal of Rock Mechanics and Mining Sciences, 80, 388-401.

Hillier, S., 2006, Appendix A. Mineralogical and chemical data, in GM Reeves, I Sims, and JC Cripps eds., Clay materials used in construction: London, Geological Society, *Engineering Geology Special Publications Volume 21*, p. 449-459.

Josh, M., Clennell, B., Cauchefert, M. & Han, T. (2016). Dielectric permittivity and anisotropy of intact multi-saturated organic shales.

Rahman, H. M., Kennedy, M., Löhr, S., & Dewhurst, D. N. (2017). Clay-organic association as a control on hydrocarbon generation in shale. *Organic Geochemistry*, *105*, 42-55.

Stanek, W., & Silc, T. (1977). Comparisons of four methods for determination of degree of peat humification (decomposition) with emphasis on the von Post method. *Canadian Journal of Soil Science*, *57*(2), 109-117.

Thomsen, L. (1986). Weak elastic anisotropy. *Geophysics*, *51*(10), 1954-1966.

Sayers, C. M. (2013). The effect of kerogen on the elastic anisotropy of organic-rich shales. Geophysics, 78(2), D65-D74.

Vernik, L., & Nur, A. (1992). Ultrasonic velocity and anisotropy of hydrocarbon source rocks. Geophysics, 57(5), 727-735.

Wu, L. M., Zhou, C. H., Keeling, J., Tong, D. S., & Yu, W. H. (2012). Towards an understanding of the role of clay minerals in crude oil formation, migration and accumulation. *Earth-Science Reviews*, *115*(4), 373-386.